Probing fractal spatiotemporal inhomogeneity in a quantum walk

Marcelo A. Pires [1,*] Caio B. Naves [2,3,†] Diogo O. Soares-Pinto [2,‡] and Sílvio M. Duarte Queirós [4,5,§]

[1]*Universidade Federal de Alagoas, 57480-000, Delmiro Gouveia-AL, Brazil*
[2]*Instituto de Física de São Carlos, Universidade de São Paulo, CP 369, 13560-970, São Carlos-SP, Brazil*
[3]*Department of Physics, Stockholm University, AlbaNova University Center, 106 91 Stockholm, Sweden*
[4]*Centro Brasileiro de Pesquisas Físicas, Rua Dr Xavier Sigaud 150, 22290-180, Rio de Janeiro-RJ, Brazil*
[5]*National Institute of Science and Technology for Complex Systems, 22290-190, Rio de Janeiro-RJ, Brazil*

We investigate the transport and entanglement properties exhibited by quantum walks with coin operators concatenated in a space-time fractal structure. Inspired by recent developments in photonics, we choose the paradigmatic Sierpinski gasket. The 0-1 pattern of the fractal is mapped into an alternation of the generalized Hadamard-Fourier operators. This two-state coin-operator approach overcomes the intricacies caused by the utilization of high-dimensional coin operators required in prior studies of discrete-time quantum walks on fractals. In fulfilling the blank space on the analysis of the impact of inhomogeneity in quantum walk properties, specifically, fractal deterministic inhomogeneity, our results show a robust effect of entanglement enhancement as well as an interesting road to superdiffusive spreading with a tunable scaling exponent attaining robust superdiffusion, subballistic though. Explicitly, with this fractal approach it is possible to obtain an increase in quantum entanglement with reduced impact on standard quantum walk theoretical spreading. Alongside those features, we analyze further properties such as the degree of interference and visibility. The present model corresponds to an application of fractals in an experimentally viable setting, namely, the building block for the construction of photonic patterned structures.

I. INTRODUCTION

Scale invariance, i.e., the intuitive sense of indistinguishability between the overall shape of several natural systems and a portion of them, has marveled humankind since a long time. Ultimately, this paved the way to the concept of fractals, either self-similar or self-affine, i.e., objects whose capacity and Lebesgue covering dimension are different from one another. Aside from its inherent beauty, fractality has found its place at the first tier of science and technology [1–3]. The endeavor to set forth fractal theory applications in the development of new scale-invariant structures can be gauged by the amount of literature that has been produced in recent years. For instance, it was shown it is possible to use molecular self-assembly to engineer an artificial nanometer-scale Sierpinski hexagonal gasket [4], structures such as Peano, Greek cross, and the Vicsek constructions to build stretchable electronic devices

with unusual mechanics [5]. Nonetheless, fractals went deep into the quantum realm by the assembling of artificial architectures of electrons with fractal geometry [6,7]. Such studies allowed the experimental investigation of subjects that have been studied only from a theoretical perspective for long.

Quantum walks (QW) [8] are the celebrated proxy lattice models for studying wave-packet spreading. Within the scope of homogeneous QWs, it is well known the emergence of interesting properties such as ballistic spreading with a non-Gaussian bimodal probability distribution that are both very distinct from the classical random walk. Still, a richer phenomenology comes up when new ingredients are introduced in the coin [9–15] or step [16–22] operators.

On the one hand, temporal inhomogeneity in QWs can be implemented by breaking the time independence of the walk operators while keeping their spatial translation invariance [13,23–28]. On the other hand, spatial inhomogeneity in QWs can break the lattice constancy of the walk operators without changing their time invariance [29–34]. A third type of inhomogeneity, the focus of our work, involves breaking both space and time constancy of the walk operators. In a comprehensive study [35], it was shown that spatiotemporal randomness embedded in the coin operator promotes the transition to a classical-like spreading in quantum walks. Other works, namely Refs. [10,36], confirmed such findings, where it was noticed that random spatiotemporal inhomogeneity leads to a slowing down in the wave-packet spreading. In Ref. [37], it was found that carefully devised nonrandom space-time inhomogeneity can be used as a probability

*marcelo.pires@delmiro.ufal.br
†caio.naves@alumni.usp.br
‡dosp@ifsc.usp.br
§sdqueiro@cbpf.br

distributions universal generator. Particularly, in Ref. [38], it was introduced a method to create spatiotemporal dependence in the coin operator that is able to display an exact classical-like binomial distribution without randomness. Those works naturally lead to the question of what dynamics should emerge if the coin operator is embedded in a deterministic space-time inhomogeneity tailored with nontrivial patterns such as fractals.

Although fractals can emerge as the output of a QW dynamics [39,40], we are going to deal with fractals the other way around, namely, as the input in the modeling process and relate it to previous works as follows: in Refs. [41–45] the focus was the problem of quantum search and in Ref. [46] it was conducted an experimental work on continuous-time quantum walks in fractal photonic lattices whereas in Ref. [47] the goal was to study the scaling of the spreading by considering a flip-flop shift operator with a four-dimensional Grover coin. In complement, the authors of Ref. [48] studied a discrete-time quantum walk (DTQW) with a two-dimensional coin operator with space dependence prescribed by the Cantor set and Sierpinski fractals were considered in a protocol of a continuous-time quantum walks (CTQWs) [49,50]. Explicitly, we take a different road by considering a theoretical proposal very close to recent experimental setups by considering a discrete-time QW with two-state coins where the fractals model a spatiotemporal alternation between generalized Hadamard and Fourier coin operators.

In this work, we present a theoretical investigation of position- and time-dependent quantum walks with fractals that are attainable in experiments with newly developed photonic architectures. Its implementation is also simpler due to the two-state nature of the coin operator, which subdues the need for introducing high-dimensional coin operators as we have aforementioned. The remaining of this paper is organized as follows: in Sec. II we introduce our DTQW model with fractal inhomogeneities; in Sec. III we present our numerical results and analytical considerations about spreading of the wave packet, the degree of interference, the entanglement entropy, and the trace distance between time-consecutive coin states; in Sec. IV we discuss the results in light of the state of the art; and finally in Sec. III we address the final considerations and further perspectives on our work.

II. MODEL

A. $1D + 1$ quantum walk

Our model is constituted in such a manner that at a given time $t \in \mathbb{N}$ we can write the quantum walker's full wave function Ψ_t as

$$\Psi_t = \sum_{x \in \mathbb{Z}} |x\rangle \otimes \psi_t(x), \tag{1}$$

$$\psi_t(x) = \psi_t^U(x) |U\rangle + \psi_t^D(x) |D\rangle, \tag{2}$$

where $\psi_t^{U,D}(x)$ are the time- and site-dependent amplitudes of probability associated with the internal degree of freedom, the coin state, $c = \{U, D\}$.

The temporal evolution proceeds with the iterative application of the operator $\widehat{W}$ as

$$\Psi_t \xrightarrow{\widehat{W_t}} \Psi_{t+1}, \tag{3}$$

$$\widehat{W}_t = \widehat{T}(\widehat{R}_t \otimes \mathcal{I}_{\mathbb{Z}}), \tag{4}$$

with the identity operator $\mathcal{I}_{\mathbb{Z}} = \sum_{x \in \mathbb{Z}} |x\rangle\langle x|$. The remaining operators that compose it are as follows:

(i) The coin operator that leaves each internal state $\{U \text{ or } D\}$ in a weighted superposition $\widehat{R}_t = \sum_x |x\rangle\langle \otimes|\widehat{R}_t(x)$, with

$$\widehat{R}_t(x) : \begin{cases} |x, U\rangle \to c_{UU}(x, t)|x, U\rangle + c_{DU}(x, t)|x, D\rangle, \\ |x, D\rangle \to c_{UD}(x, t)|x, U\rangle + c_{DD}(x, t)|x, D\rangle, \end{cases} \tag{5}$$

where $c_{ij}(x, t)$ are the elements of the rotation matrices playing the role of quantum walk coins used in our study: the biased Hadamard coin operator $\widehat{C}_H(\theta_H)$ and the biased Fourier coin operator $\widehat{C}_F(\theta_F)$ mathematically described by

$$\widehat{C}_H = \begin{pmatrix} \cos\theta_H & \sin\theta_H \\ \sin\theta_H & -\cos\theta_H \end{pmatrix},$$

$$\widehat{C}_F = \begin{pmatrix} \cos\theta_F & i\sin\theta_F \\ i\sin\theta_F & \cos\theta_F \end{pmatrix}. \tag{6}$$

(ii) The spin-dependent displacement operator that splits the wave packet towards $\pm x$:

$$\widehat{T} : \begin{cases} |x, U\rangle \to |x + 1, U\rangle, \\ |x, D\rangle \to |x - 1, D\rangle. \end{cases} \tag{7}$$

B. The Sierpinski gasket concatenation of optical elements

As already mentioned, herein we center our attention on the impact of one of the canonical instances of self-similarity, the Sierpinski gasket (SG). It corresponds to a fractal with (equilateral) triangle external contour shape obtained by means of the recursive division of a first triangle into ever smaller triangles. Geometrically, it corresponds to starting with an equilateral triangle that is divided into four congruent smaller equilateral triangles with half the size and the removal of the central triangle. Analyzing it the other way around, i.e., from a zooming-out perspective, we understand that in doubling the size of a triangle the Sierpinski generator creates three replicas of the previous triangle. That allows finding the fractal dimension of the nonrandom pattern,

$$d_f = \frac{\ln(\text{number of replicas})}{\ln(\text{resize factor})} = \frac{\ln 3}{\ln 2} = 1.58\ldots, \tag{8}$$

which is less than the Lebesgue covering dimension $D = 2$ but greater than the dimension of a line, $d = 1$. Formal aspects of this matter can be found in Refs. [1,51].

Scale invariance mainly splits into two classes: when we are dealing with homogeneous dimensions and when the fractal spans through different dimensions such as space and time. In the former case we refer to self-invariance whereas in the latter we are dealing with self-affinity. In respect thereof, the Sierpinski gasket is obtained not only using geometrical arguments, as we have stated, but it is the space-time outcome of several dynamical models as well. Aside from the celebrated Rule 90 of cellular automata [52], as well as a plethora of other
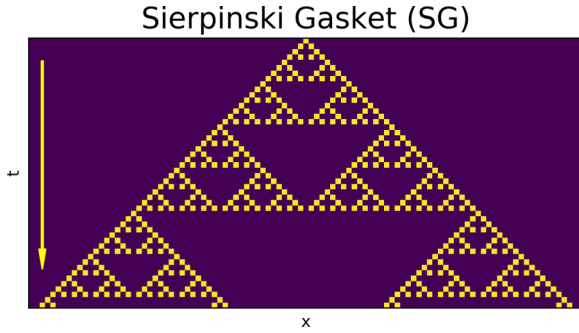
Sierpinski Gasket (SG)

FIG. 1. Sierpinski gasket (SG). In this binary carpet yellow indicates the value 1 that corresponds to the application of the operator $\widehat{C}_H$. The other sites inside the largest yellow triangle indicate the value 0 that corresponds to the application of the operator $\widehat{C}_F$. In this way it is possible to build a fractal assembly of optical elements.

algorithms [53], the space-time SG can be obtained by means of the next fast modular arithmetic rule [54]

$$b_t(x) = [b_{t-1}(x-1) + b_{t-1}(x+1)] \mod 2, \qquad (9)$$

where $b_t(x)$ is a site- and time-dependent binary $\{0, 1\}$ variable. At first glance, Eq. (9) seems to be linear, but a closer look reveals that the modular arithmetic that constrains $b_t(x)$ to either 0 or 1 introduces nonlinearity. In Fig. 1, we present $t = 50$ generations of the SG. From Eq. (9) it is clear that inside the cone $-t \leqslant x \leqslant t$ there is only $0-1$.

We are now in the condition of using the self-similarity seasoning of our work into the quantum walk dynamics by defining the quantum operator

$$\widehat{R}_t(x) \equiv b_t(x)\widehat{C}_H + (1 - b_t(x))\widehat{C}_F. \qquad (10)$$

This equation reads as whenever a given site has $b_t(x) = 0$ we set $\widehat{C}_F$ and whenever $b_t(x) = 1$ we set $\widehat{C}_H$. That establishes an important difference between our model and other photonic transport work; specifically, in the system we study the fractal element resides within the coin operator selector whereas in other cases the fractal element has to do with the physical geometry of the grid (see, e.g., Ref. [46]). Overall, we understand the present model as a space-time inhomogeneous model and such traits will be taken into consideration in the interpretation of the results.

As a matter of clarification, we must stress that despite that the position and internal state of the walker are randomly determined through measurement, the quantum walk evolution that we just described is a deterministic one, in the same way as the standard discrete-time quantum walk protocol. Given that the fractal pattern is obtained by a fixed rule, the coin operators that are in turn determined by the fractal, although being inhomogeneous in space and time, also follow a deterministic rule. This differs from other types of quantum walk protocols that while they are composed through unitary operators each of them are determined through a probabilistic rule, for instance, where the coin operators [9,10] or where the shift operators [17,18] are determined randomly in each time step, making the whole evolution a random one.

With respect to the initial condition, we have placed the starting point of the QW at the same initial location of the seed in the fractals. For the boundary conditions, we have

established that for each t we worked with an augmented chain of positions so that the quantum walker was not able to reach the boundaries. Instances of the quantum walk as established by our dynamics are provided in Fig. 2.

Taking an experimental-friendly setup, we consider the proposals in Refs. [55,56], where the role of the coin operators is played by beam splitters and the internal degree of freedom $c = \{U, D\}$ is the polarization of the photons. While $\widehat{C}_F$ leaves each state in a superposition with an additional phase, $\widehat{C}_H$ produces a superposition of states without such extra phase. If $\theta = \pi/4$, we recover the standard Hadamard and Fourier coin operators that can be implemented with an unbiased beam splitter.

III. RESULTS

In this section, we will present our results regarding the transport properties of the quantum walk, as well as the degree of interference, entanglement entropy, and trace distance between time-consecutive coin states.

A. Spreading

At a given instant t, we compute the probability

$$P_t(x) = |\psi_t^D(x)|^2 + |\psi_t^U(x)|^2. \qquad (11)$$

That is of experimental interest for it allows obtaining preliminary assessment of the wave-packet transport properties. For each t, we also have computed $P_t^{\max}$ that is the maximum of $P_t(x)$ over the chain.

At this point we must mention that in the standard quantum walk evolution, which is with a spatiotemporal invariant coin operator, it is possible to find the walk time-asymptotic properties through the Schrödinger approach [57–59]. This method consists in analyzing the evolution in momenta space, where a diagonalizable evolution operator is found. Then, we are able to find the time-asymptotic state and therefrom its properties by taking the proper limit t going to infinity. However, in our proposed QW the evolution operator loses its invariance by pairing the Sierpinski fractal with the coin operator, which makes such sort of treatment impracticable. Therefore, all the following results are obtained through numerical calculations.

In Fig. 2 we plot the normalized profile $P_t(x)/P_t^{\max}$ for the typical angles $\theta = \{15°, 45°, 75°\}$, where we immediately note that the standard QW (upper panel) already displays a trianglelike shape. That signals the overwhelming majority of the flux of probability is near the edges. Such a feature accommodates well our proposal for implementing QW through the Sierpinski triangle (ST). In the homogeneous setting, we also see that the smaller the value of θ, the broader the wave packet. This is because the mathematical structure of the coin operators favors the terms c_{UU} and c_{DD} in Eq. (10), which are related to spreading. However, this property is modified when the flux of probability passes through the SG. The profiles of $P_t(x)$ are neither bimodal-like distribution nor a Gaussian-type shape. In other words, the intrinsic nonlinearities of the fractals leaves peculiar fingerprints in the wave packet. Even though the SG is symmetric, there are clear asymmetries in $P_t(x)$ due to the swinging between the coin operators that give different phases to the local spinor (2).
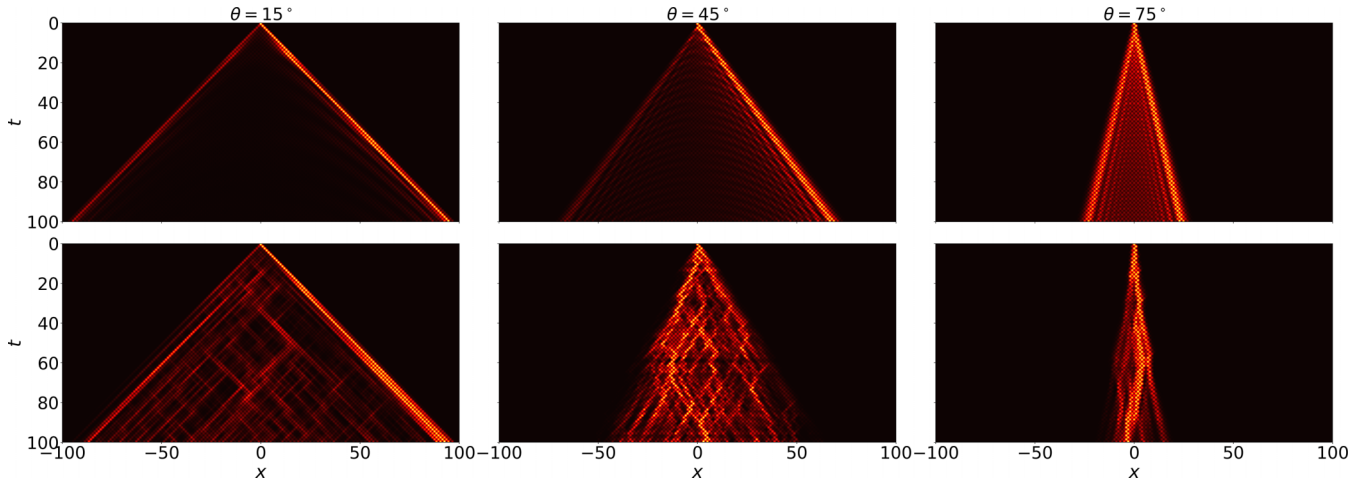
FIG. 2. Space-time evolution of the normalized probability distribution $P_t(x)/P_t^{\max}$ where the brightness denotes the magnitude of this quantity. Quantum carpets for the homogeneous setting (upper panels) and inhomogeneous cases (lower panels). We set with $t_{\max} = 100$ and $\theta = \{15°, 45°, 75°\}$.

The qualitative information obtained by the visual inspection of the quantum carpets presented in Fig. 2 is quantitatively boosted by computing the second statistical moment

$$m_2(t) = \overline{x^2}_t = \sum_x x^2 P_t(x), \tag{12}$$

from which we get the scaling exponent

$$\alpha = \lim_{t \to \infty} \frac{\log_{10} m_2(t)}{\log_{10} t}, \tag{13}$$

that defines the sort of diffusion the system presents. For $0 < \alpha < 1$, a system is subdiffusive; $\alpha = 1$ corresponds to standard diffusion (similar to the classical random walk); when $1 < \alpha < 2$, it exhibits superdiffusion; for $\alpha = 2$, we have ballistic diffusion like the standard QW and for $\alpha > 2$ a system runs in a superballistic regime with the particular value $\alpha = 3$ corresponding to hyperballistic diffusion [17].

In Fig. 3, we understand that the nonrandom fractal inhomogeneity fails to make the scaling exponent decrease to the level of the diffusive behavior $\alpha = 1$, as happens for random spatiotemporal assembly of coin operations [35]. Therefrom, we perceive a nonmonotonic and nonsmooth dependence of α with θ that arises from substantial enhancement of the interference between the paths along the time evolution caused by the fractal infrastructure as previously shown in Fig. 2. This nonmonotonicity is an intriguing feature if we take into account the overall regularity in the patterns through the SG.

The behavior of α with θ is shown in Fig. 4. In the standard QW it is well known that changing θ alters the particular features of $m_2(t)$ while keeping the scaling exponent α invariant. Here, our results show that by tuning θ it is possible to slightly change (and with statistical significance) the level of superdiffusivity of the quantum walker, still below the ballistic regime though. This result, the dependence of α with θ, is absent in all the previous endeavors working with coined QWs on fractals [41–45,47–50]. Indeed, with the present proposal it is possible to adjust $\theta = m\pi$ ($m \in \mathbb{N}$) in order to obtain a spreading that is substantially close to $\alpha = 2$. Namely, allowing for the

current experimental state of the art, this spreading behavior would effectively overlap that obtained from ballistic quantum walk implementations within error bars; see, e.g., Fig. 4 in [56] where $\alpha = 2$ is assumed simply.

In complement, this setup can be interpreted from the perspective of the physics of inhomogeneous systems [3,51]. Space-time inhomogeneity is not only of theoretical interest, but it has been shown in optical systems that they are able to produce a remarkably new phenomenology as well [60]. The results in Figs. 3 and 4 highlight the emergence of a mechanism to access the superdiffusive regime, which is an important class of anomalous diffusion on its own [61].

On the whole, the results depicted in Figs. 2–4 show that a fractal assembly of coin operators leads to a rich phenomenology in terms of wave-packet spreading, even when the coin
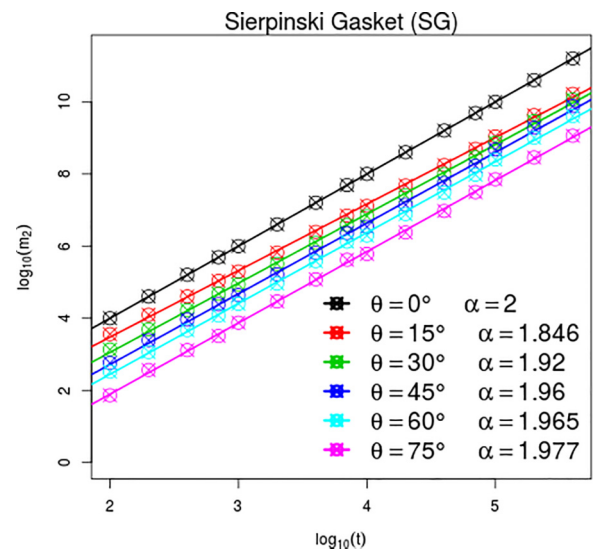

FIG. 3. Temporal behavior of the spreading measure m_2 in a $\log_{10}$ - $\log_{10}$ scale. Data points are the results from simulations and the lines are linear fittings.
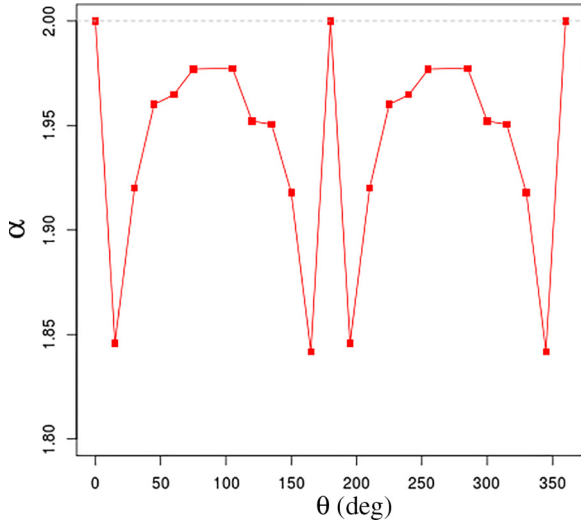
FIG. 4. Diagram α vs θ. We use $t_{\max} = 5 \times 10^5$ to estimate α from $m_2 \sim t^\alpha$. The case $\theta = m\pi/2$ with $m = \{1, 3, 5\}$ is not shown because it leads to a bounded behavior that leads to $\alpha = 0$ (non-spreading) corresponding to specious localization.

operators differ only by mere phase factors as explicit in the operators $\widehat{C}_H$ and $\widehat{C}_F$ shown in Eq. (6).

B. Degree of interference

As a means to study with more detail the interference effects between the different paths that come up with different dynamics of the walker in this setup, we have also investigated the degree of interference. The degree of interference is defined as the norm of the quantity responsible for the interference in the visibility pattern. The visibility, in turn, suitable for probability waves is defined as

$$\mathcal{V}(x, t) \equiv \frac{\max[P_t(x)] - \min[P_t(x)]}{\max[P_t(x)] + \min[P_t(x)]}. \qquad (14)$$

Then, the degree of interference at each position and time step is defined as the norm of the numerator of the visibility. For further details on how we calculated this quantity in the quantum walk with fractal inhomogeneity see Appendix, Sec. A 1:

$$\mu(x, t) = |\max[P_t(x)] - \min[P_t(x)]|. \qquad (15)$$

In Fig. 5, we have the degree of interference at each position as a function of time for the same evolution represented at Fig. 2 in the second row, i.e., the inhomogeneous case. There,

it is possible to see that the interference pattern evolution closely follows that of the probability distribution; in other words, the plot tells us that at each site the interference occurs between its immediate neighbors, as one would expect from the short-range coupling of the quantum walk step evolution.

By investigating how the degree of interference behaves as a function of the coin operators [Eq. (6)], we also found some interesting patterns that resemble the fractal structure used to implement the inhomogeneous coin operator [Eq. (10)] as shown in Fig. 6. These patterns arise when we set the Fourier coin operator to be equal to the identity, i.e., $\theta_F = 0$, and we start with a coin initial state parametrized by the angles on the Bloch sphere

$$\psi_0(0) = \cos\frac{\gamma}{2} |U\rangle + e^{i\phi} \sin\frac{\gamma}{2} |D\rangle, \qquad (16)$$

with angles $\gamma = \pi/2$ and $\phi = 0$.

One can understand why the pattern resembles a SG fractal by recalling the definition of the degree of interference, Eqs. (A11) and (A13), with the arithmetic rule used to generate the pattern (9). From Eq. (A11) we note that for the degree of interference to be nonzero at a given position, at least one of the coin operators applied in its immediate neighbors' positions in the previous time instant must be different than the identity operator $\widehat{C}_F(\theta_F = 0)$, i.e., $R_{t-1}^{UD} \neq 0$ and/or $R_{t-1}^{DU} \neq 0$. This matches with the sum modulus two where, if $b_{t-1}(x \pm 1)$ are both zero, then $b_t(x) = 0$. Moreover, one must have a coin in a superposition state, that is $c_U(x + 1, t - 1), c_D(x + 1, t - 1) \neq 0$ and/or $c_U(x - 1, t - 1), c_D(x - 1, t - 1) \neq 0$. The lack of a superposition can come from the application of an identity operator in a state previously in a basis state or from the application of $\widehat{C}_H$ in one coin at $x + 1$ or $x - 1$. That means when we have $\widehat{C}_H$ acting on both the coin states at $x \pm 1$ the interference degree can be zero or nonzero, based on the prior states at these positions, and when $\widehat{C}_H$ acts on either of them the outcome is the same. That differs from the sum modulus two rule (9) that states when both $b_{t-1}(x \pm 1)$ are equal to one, then $b_t(x) = 0$ and when only one of them is equal to one, $b_t(x) = 1$. Still, we can affirm that the pattern closely resembles the SG fractal for the reason that the majority of points are zero, imposing that the intermediate points in the future are also zero. We also emphasize the dependence of the pattern on the coin initial state [compare Fig. 6(a) with Fig. 6(f)]. Given that one has a small θ_H, then one of the components of the coin state in a given position can be made smaller, resulting in a smaller interference for the points that should be zero and not for the ones that should not. In the Appendix, Sec. A 2, we show an analytical calculation of the
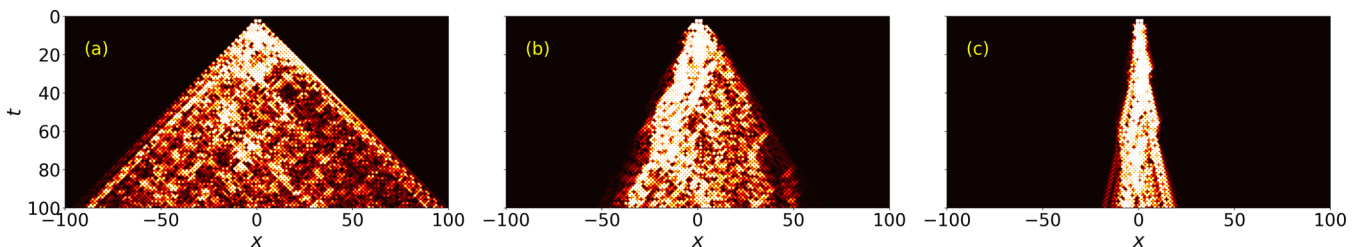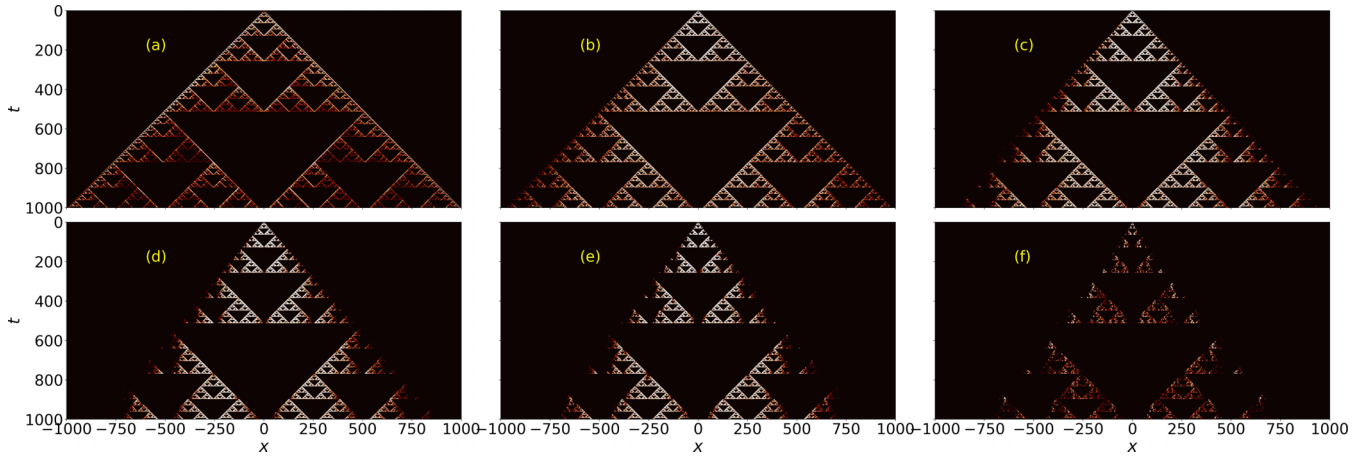

FIG. 5. Degree of interference spatial-temporal evolution in the walks following the same parameters of the lower panels (inhomogeneous cases) in Fig. 2: (a) $\theta_H = \theta_F = 15°$, (b) $\theta_H = \theta_F = 45°$, and (c) $\theta_H = \theta_F = 75°$.

FIG. 6. Degree of interference spatial-temporal evolution in walks with $\theta_F = 0°$ initially localized in the origin with coin initial state parameters $\gamma = \pi/2$, $\phi = 0$. In (a) $\theta_H = 5°$, (b) $\theta_H = 15°$, (c) $\theta_H = 30°$, (d) $\theta_H = 45°$, (e) $\theta_H = 60°$, and (f) $\theta_H = 85°$.

initial steps of the degree of interference evolution in Fig. 6 for any θ_H.

C. Entanglement entropy

To quantify the amount of entanglement generated through the position-coin system we have employed the entanglement entropy

$$S_E \equiv -\mathrm{tr}(\rho \, \log_{10} \rho), \qquad (17)$$

where ρ is the density operator of the system. Here, we focus only on the entropy of the coin subsystem. As we are treating a two-level system, the entanglement entropy varies between $0 \leqslant S_E \leqslant 1$, with zero corresponding to a separable state and with one to a fully entangled state, and it is given by

$$S_E = -\lambda_+ \log_{10} \lambda_+ - \lambda_- \log_{10} \lambda_-, \qquad (18)$$

with $\lambda_\pm$ being the eigenvalues of the coin density operator ρ_c.

Since the evolution of the coin entanglement entropy in a quantum walk often presents an initial increase to then stabilize around a given saturate value, we consider the time-average entanglement entropy in the asymptotic regime, $t \geqslant t_0 \gg 1$. The time evolution of the entanglement entropy also depends on the coin initial state and coin operator used. Therefore, we take the initial time after which we can consider the regime as being a quasistationary one, t_0, based on each evolution.

We start by analyzing the coin entanglement entropy as a function of the coin operator parameters [Eq. (6)] θ_H and θ_F in Fig. 7 with a density plot view of it in Fig. 8. The coin initial state considered is the one with $\phi = \gamma = \pi/2$ in the qubit Bloch-sphere equation (16) and localized at the origin. Figure 7 shows us that the entanglement entropy reaches its maximum value for the set of parameters with $\theta_F \lesssim 85°$, which is almost the entire set of parameters. For $\theta_F = 90°$, the maximum value is obtained with $\theta_H = 0°$, after which it starts to decay and reach the minimum value of $\overline{S_E} \approx 0.498$ with $\theta_H = 90°$ (Fig. 9). This is an interesting feature since it does not happen in the standard quantum walk evolution. Moreover, a similar effect was reported for other types of inhomogeneous quantum walk, with the inhomogeneity also in

the coin operation and in the shift operator [9,18,33,36]. However, all of them impose a random quantum walk evolution whereas in the present model the evolution is deterministic. The presence of temporal inhomogeneity in the evolution of those walks is the key factor leading to the same phenomenon, as was asserted in [22,36].

When we have fixed the coin operators to be the ones with $\theta_H = \theta_F = \pi/4$, we observed that by varying the coin initial state angles the entanglement entropy averaged over time is independent of the entire set of parameters. That is indicative of the robustness of the generation of entanglement between the coin and position states with regard to changes in the initial state [19].

D. Asymptotic regime

Next, we probe how the coin state evolves towards its time-asymptotic regime. To that, we employ the trace distance measure

$$D(\rho, \sigma) = \tfrac{1}{2} \| \rho - \sigma \|_1, \qquad (19)$$

where $\|A\|_1 = \mathrm{tr}(\sqrt{A^\dagger A})$. If a quantum system is evolving in a stationary regime, its density operator does not change with time, $\rho(t + \Delta t) = \rho(t)$, therefore, the trace distance between $\rho(t + \Delta t)$ and $\rho(t)$ would return zero. In this way we see how the trace distance between two time-consecutive states evolves.

Initially, we fix one of the parameters of the coin operator $\theta_H = \pi/4$ in Fig. 10(a). There, we can see that for all θ_F but $\theta_F = 0$, the trace distance decays essentially in the same way. The inset gives us the log-log graph of the same curves with the respective linear fittings yielding the decay exponents if $D(\rho_c(t+1), \rho_c(t)) \propto t^{-\beta}$, confirming this observation.

When we fix the other coin operator with $\theta_F = \pi/4$ [Fig. 10(b)], the evolution with $\theta_H = 0$ does not decay as fast as in the case where $\theta_F = 0$ in Fig. 10(a), with $\beta \approx 0.59$. For the remaining angles, the decay rates are essentially the same with the exception of $\theta_H = \pi/2$ that gives us $\beta \approx 0.08$. At this angle something interesting happens: the trace distance does not decay, on average, monotonically, having intervals of constant evolution with some increases in-between.
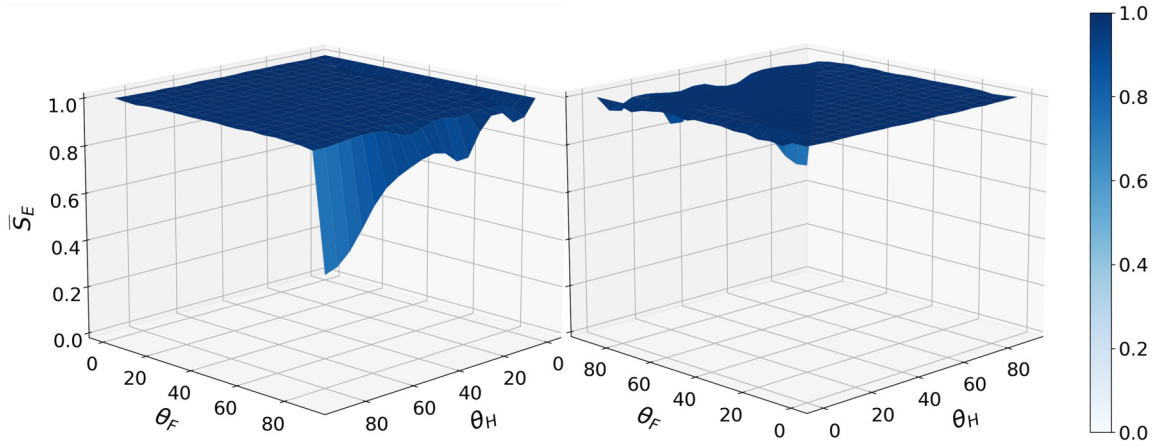
FIG. 7. Time-average coin entanglement entropy in the asymptotic regime as a function of the parameters of the two possible coin operators [Eq. (6)] θ_H (deg) and θ_F (deg), respectively. The initial state considered was the one with $\phi = \gamma = \pi/2$ with the initial position in the origin, $x_0 = 0$. For $\theta_H = \theta_F = 0$ is $S_E = 1$.

Figure 11 shows the time evolution of the trace distance between two consecutive coin states when we set the coin operators to be the those with $\theta_H = \theta_F = \pi/4$ and change the coin initial state. In Fig. 11(a), the polar angle is set $\gamma = \pi/2$ while we change the phase angle ϕ. We see that changes in this parameter do not change the trace distance decay behavior, on average, giving us essentially the same decay exponent $\beta \approx 0.66$ for $\phi = \{0, \pi/6, \pi/4\}$ with the most divergent, but still very close, $\beta \approx 0.57$ for $\phi = \pi/2$. Setting $\phi = \pi/2$ and changing γ, Fig. 11(b) demonstrates that changes in this parameter also do not change the trace distance decay significantly, now even when we set $\gamma = \pi/2$. From both Figs. 10 and 11 we observe a decay law compatible with an effective stationary behavior, i.e., stationary on average and within a fluctuation band, validating the time average taken on the von Neumann entropy analysis.

These results tell us that despite our quantum walk model being inhomogeneous, it goes to the quasistationary regime
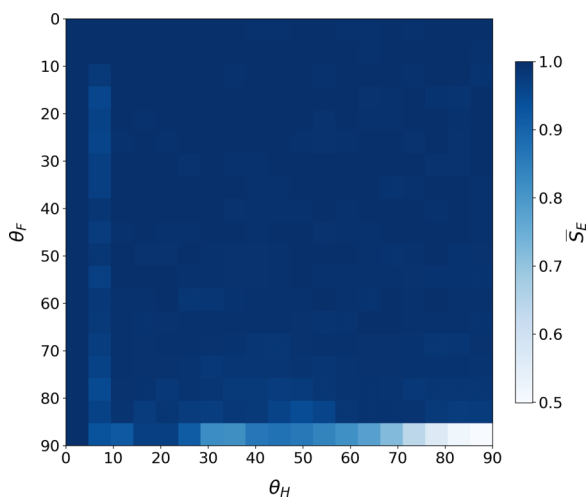

FIG. 8. Two-dimensional display of the time-average entanglement entropy as a function of θ_H (deg) and θ_F (deg) data used to plot Fig. 7.

essentially in the same way as if we had fixed the coin operators and changed the coin initial state and vice versa, excluding the cases where the parameters are near to $\pi/2$. This is strongly indicative that this property derives from the quantum walk protocol and only has a small limited dependence on the initial conditions. In the standard Hadamard walk, the pace at which the coin state converges to the stationary regime depends on the initial state and coin operator used. Comparing with other types of inhomogeneous quantum walks, we see that the introduction of a fractal inhomogeneity in the coin operator induces a faster transition to the stationary regime with $\beta \approx 0.55$ than when one introduces a dynamically and fluctuating randomness [9,36], where the decay exponent $\beta = \frac{1}{4}$. For walks with a weak inhomogeneous condition between the Fourier and Hadamard coin operators [62], something similar to our proposal, the coin state is also led to converge faster to the asymptotic limit. The decay exponent of the walk with fractal inhomogeneity is also greater than the ones in the generalized elephant quantum walk, where the randomness is on the step sizes and selected according to the q exponential, when its parameter q is less than one but greater than half, $\beta(q) \approx \frac{1}{4}$, but in the uniform distribution limit $q \to \infty$ it becomes smaller, where $\beta(q) \approx 0.76$.

IV. DISCUSSION

Within the context of quantum walks, the inhomogeneity of our Sierpinski gasket case befalls twofold: every site of the grid is associated to a given coin operator protocol that is updated at each time step according to the dynamics (9). On the one hand, it is known that the slightest spatial inhomogeneity induces an absence of diffusion and the subsequent localization of the quantum walker wave; on the other hand, temporal randomness can actually enhance spreading of the wave packet, especially when such changes occur at typically long timescales [55]. Thus, taking into consideration this model has spatial inhomogeneity, we would expect a dramatic decrease of the exponent α, which is not the case. As shown, the system preserves a level of diffusion not far from the
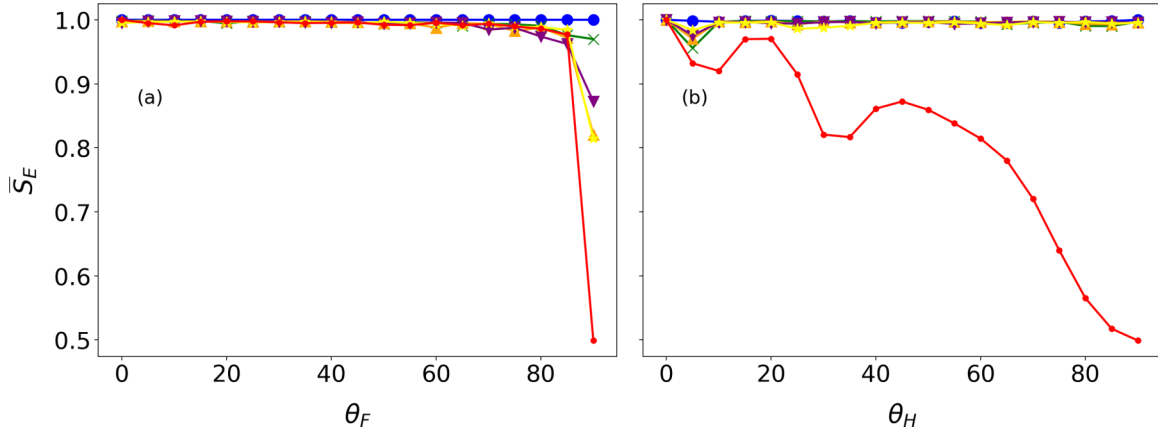
FIG. 9. Time-average coin entanglement entropy as a function of θ_F(deg) (a) and as a function of θ_H(deg) (b). Each curve corresponds to the following values for the other coin operator parameter, $\theta_H(a)$, θ_F (b), with 0° (blue circle), 15° (green cross), 30° (orange up triangle), 45° (purple down triangle), 60° (yellow star), and 90° (red dot).

standard ballistic behavior with mild dependence on the angle of the coin. In order to understand that, we have inspected the local statistics of coin operator updates. Excluding the central grid site $x = 0$, we have verified that the average time for coin change τ_x is never less than a two-digit figure, with that average time increasing with $|x|$, namely, $\tau_5 = 74$, $\tau_{30} = 146$, $\tau_{100} = 219$. Combining both elements, we understand the long characteristic scale of the coin dynamics manages to zero out to a large extent the likely localization that would be induced by static inhomogeneity. At the same time, we have verified the effect of spatial inhomogeneity in augmenting quantum entanglement [33] (excluding the particular coin-operator

angles such as $\theta = 90$), which is lessened by the temporal inhomogeneity effects of the dynamics (9). In other words, we have verified that deterministic fractal inhomogeneity enhances quantum entanglement without achieving the maximal value though. It is precisely that deterministic nature of the self-similar fractal dynamics that reins in quantum entanglement strengthening, as previously hinted [9]. That said, we can particularly envisage this type of architecture as a strong candidate for tailored problems for which one aims at increasing entanglement while ensuring a high level of spreading, e.g., search algorithms in a quantum cryptography environment [63].
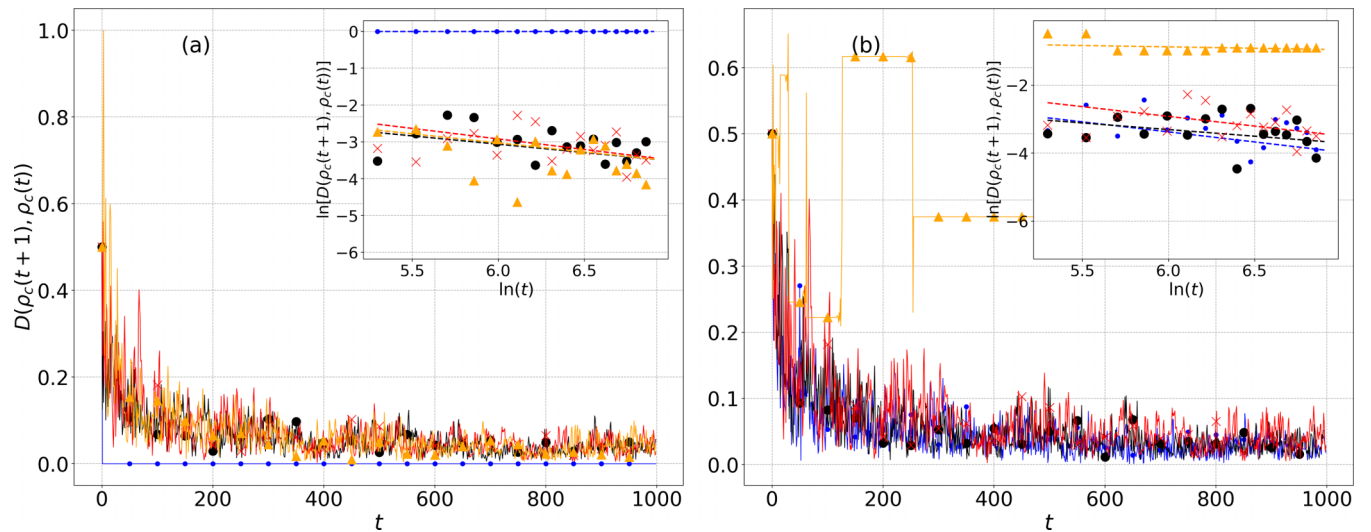

FIG. 10. Trace distance between time-consecutive coin states as a function of time for (a) different θ_H, with $\theta_F = \pi/4$, and (b) different θ_F with $\theta_H = \pi/4$. The different angles used in each plot follow the colors and patterns 0 (blue dotted), $\pi/6$ (black circled), $\pi/4$ (red crossed), and $\pi/2$ (orange up triangle). In each evolution a localized initial state was considered with coin initial state parametrized by $\phi = \gamma = \pi/2$. The insets indicate the log-log graph of the same plots with linear fittings of the form $-\beta \ln(t) + \alpha$. For (a) we have the following angular and linear coefficients: $\beta = 0.00 \pm 0.00$, $\alpha = 0.00 \pm 0.00$ (blue dotted); $\beta = 0.45 \pm 0.04$, $\alpha = -0.4 \pm 0.3$ (black circled); $\beta = 0.57 \pm 0.04$, $\alpha = 0.5 \pm 0.3$ (red crossed); $\beta = 0.49 \pm 0.04$, $\alpha = -0.1 \pm 0.3$ (orange up triangle). For (b) we have the following ones: $\beta = 0.59 \pm 0.05$, $\alpha = 0.2 \pm 0.03$ (blue dotted); $\beta = 0.39 \pm 0.04$, $\alpha = -1.0 \pm 0.3$ (black circled); $\beta = 0.57 \pm 0.04$, $\alpha = 0.5 \pm 0.3$ (red crossed); $\beta = 0.08 \pm 0.04$, $\alpha = -0.39 \pm 0.06$ (orange up triangle).
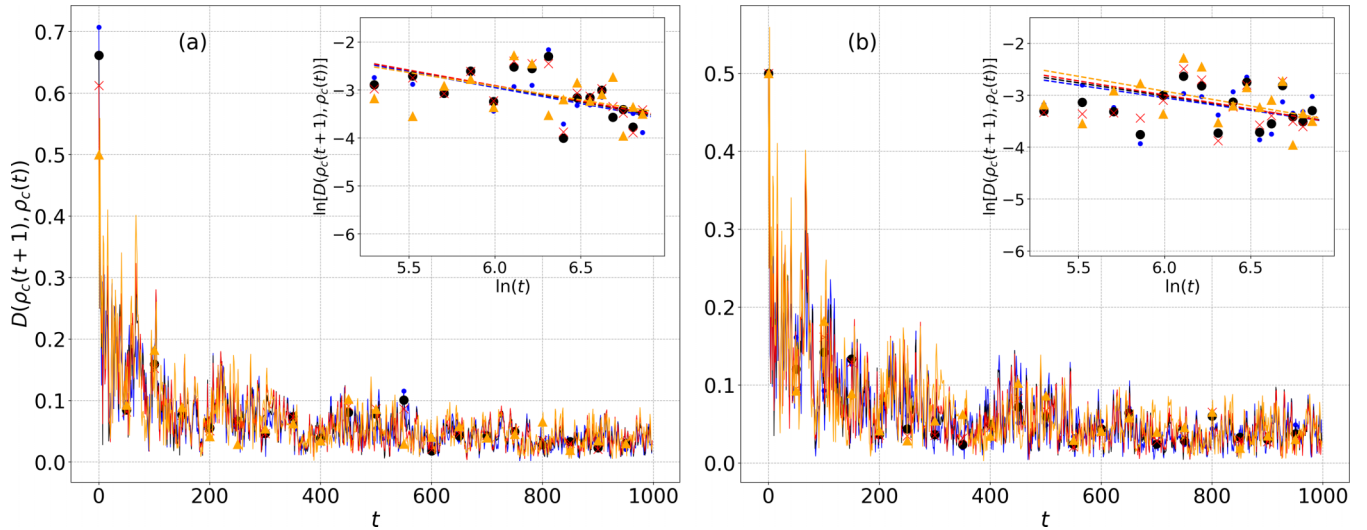
FIG. 11. Trace distance between time-consecutive coin states as a function of time for different angles of the coin initial state Bloch sphere ϕ (a), with $\gamma = \pi/2$, and different γ(b) with $\phi = \pi/2$ [see Eq. (16)]. The different angles used in each plot follow the colors and patterns 0(blue dotted), $\pi/6$(black circled), $\pi/4$(red crossed), and $\pi/2$(orange up triangle). In each evolution a localized initial state was considered with coin operators given by $\theta_H = \theta_F = \pi/4$. The insets indicate the log-log graph of the same plots with linear fittings of the form $-\beta \ln(t) + \alpha$. For (a) we have the following angular and linear coefficients: $\beta = 0.67 \pm 0.04$, $\alpha = 1.1 \pm 0.3$ (blue dotted); $\beta = 0.66 \pm 0.04$, $\alpha = 1.0 \pm 0.3$ (black circled); $\beta = 0.65 \pm 0.04$, $\alpha = 1.0 \pm 0.2$ (red crossed); $\beta = 0.57 \pm 0.04$, $\alpha = 0.5 \pm 0.3$ (orange up triangle). For (b) we have the following ones: $\beta = 0.48 \pm 0.05$, $\alpha = -0.1 \pm 0.3$ (blue dotted); $\beta = 0.51 \pm 0.04$, $\alpha = 0.0 \pm 0.3$ (black circled); $\beta = 0.54 \pm 0.04$, $\alpha = 0.2 \pm 0.3$ (red crossed); $\beta = 0.57 \pm 0.04$, $\alpha = 0.5 \pm 0.3$ (orange up triangle).

V. FINAL REMARKS

In our work we have presented a quantum-walk-based fractal protocol in which it is possible to achieve an increase in quantum entanglement, accompanied by a superdiffusive regime that is able to attain values close to ballistic that can be experimentally implemented using photonic architectures and which offers alternatives for bridging fractals and photonics [64,65] in a more bold way. We have done so by employing the paradigmatic Sierpinski gasket as a prototype and explored the transport properties of that inhomogeneous quantum walk, namely, the spreading of the wave packet, the degree of interference, the entanglement entropy, and the trace distance between time-consecutive coin states.

An important advantage of our work in relation to previous proposals [42–45,47] lies in the fact that the versions of the discrete-time QWs on fractals studied in those works require the use of high-dimensional coin operators that are harder to implement. Our protocol simply considers a two-state coin. Specifically, in Ref. [42] it was used a d-dimensional coin Hilbert space. In Refs. [43–45,47] their flip-flop walk requires a four-dimensional Grover coin. Thus, the experimental feasibility of the present QW dynamics presented a clear implementable advantage; furthermore, it can be realized with the state-of-art photonics technology. Still, with minor changes in the apparatus described in Ref. [56], it is possible to implement the fractal concatenation of optical elements where the role of time t is played by the propagation direction. The nonrandom character of our proposal has the additional feasibility of not requiring an extra sampling processing over random inhomogeneity.

The employment of fractal principles in the creation of patterned structures is an avenue of research to be studied from both fundamental and applied perspectives. In this paper, we have provided an application of fractal geometry, namely, we showed that the Sierpinski gasket can be utilized to build photonic architectures aimed at realizing highly nontrivial site- and time-dependent quantum dynamics. While fractal structures were previously addressed in the scope of QWs [41–50], those efforts had different frameworks and goals than what we presented here. Accordingly, with this work where the inhomogeneity is deterministically established, we have fulfilled a gap on the characterization of the impact of different sorts of inhomogeneity on the properties of a quantum walk. Last, this contribution brings fresh insights into the physics of inhomogeneous photonics [66]. Alongside further studies on the extension of the analytical treatment in the reciprocal space for cases with this sort of inhomogeneity for which the invariance of the evolution operator is subdued, an interesting open problem to explore is how the wave-packet properties behave when a multifractal structure is brought into play to incorporate inhomogeneity in the system.

ACKNOWLEDGMENTS

APPENDIX A: THE DEGREE OF INTERFERENCE

1. Definition

In the following, we present the way we have calculated the degree of interference in connection with the proposed quantum walk model. As we mentioned previously, the degree of interference is defined as the norm of the quantity responsible for the interference in the visibility. The visibility, suitable for probability waves, is

$$\mathcal{V} = \frac{P_{\max} - P_{\min}}{P_{\max} + P_{\min}}. \tag{A1}$$

Then, the degree of interference at each position and time step is defined as the norm of the numerator of the visibility

$$\mu(x, t) = |P_{\max}(x, t) - P_{\min}(x, t)|. \tag{A2}$$

Let $|\psi(t)\rangle$ be the walker state at time t expanded as

$$\Psi(t) = \sum_x |x\rangle \otimes [c_U(x, t)|U\rangle + c_D(x, t)|D\rangle]. \tag{A3}$$

The coin operator $\hat{R}_t$ in the quantum walk is defined following the Sierpinski-gasket fractal rule so that

$$\hat{R}_t = \sum_x |x\rangle\langle x| \otimes \hat{R}_t(x), \tag{A4}$$

with $\hat{R}_t(x)$ given by Eq. (10).

Therefore, the recursive maps that provide the walker state coefficients' time evolution now are going to include the space-time-dependent coin operator factors. Let

$$\hat{R}_t(x) = R_t^{UU}(x)|U\rangle\langle U| + R_t^{UD}(x)|U\rangle\langle D| + R_t^{DU}(x)|D\rangle\langle U| + R_t^{DD}(x)|D\rangle\langle D|, \tag{A5}$$

consequently, the recursive map for the state coefficients is going to be, assigning the up state to a displacement to the right,

$$c_U(x, t+1) = R_t^{UU}(x-1)c_U(x-1, t) + R_t^{UD}(x-1)c_D(x-1, t), \tag{A6}$$

$$c_D(x, t+1) = R_t^{DU}(x+1)c_U(x+1, t) + R_t^{DD}(x+1)c_D(x+1, t). \tag{A7}$$

The position probability distribution is given by the square norm of the walker state's coefficients

$$P(x, t) = |c_U(x, t)|^2 + |c_D(x, t)|^2. \tag{A8}$$

Using the recursive relations Eqs. (A6) and (A7), we find

$$P(x, t) = \left| R_{t-1}^{UU}(x-1)c_U(x-1, t-1) + R_{t-1}^{UD}(x-1)c_D(x-1, t-1) \right|^2$$
$$+ \left| R_{t-1}^{DU}(x+1)c_U(x+1, t-1) + R_{t-1}^{DD}(x+1)c_D(x+1, t-1) \right|^2 \tag{A9}$$

$$= \left| R_{t-1}^{UU}(x-1)c_U(x-1, t-1) \right|^2 + \left| R_{t-1}^{DD}(x+1)c_D(x+1, t-1) \right|^2 \left| R_{t-1}^{UD}(x-1)c_D(x-1, t-1) \right|^2$$
$$+ \left| R_{t-1}^{DU}(x+1)c_U(x+1, t-1) \right|^2 + \left| R_{t-1}^{UD}(x-1)c_D(x-1, t-1) \right|^2$$
$$+ R_{t-1}^{UU}(x-1)\left[R_{t-1}^{UD}(x-1) \right]^* c_U(x-1, t-1)c_D(x-1, t-1)^*$$
$$+ R_{t-1}^{DU}(x+1)\left[R_{t-1}^{DD}(x+1) \right]^* c_U(x+1, t-1)c_D(x+1, t-1)^* + \text{c.c.} \tag{A10}$$

Defining the complex part as a function $f(x, t)$,

$$f(x, t) = R_{t-1}^{UU}(x-1)\left[R_{t-1}^{UD}(x-1) \right]^* c_U(x-1, t-1)c_D(x-1, t-1)^*$$
$$+ R_{t-1}^{DU}(x+1)\left[R_{t-1}^{DD}(x+1) \right]^* c_U(x+1, t-1)c_D(x+1, t-1)^*,$$

the maximum probability and the minimum probability are going to be

$$P_{\max}(x, t) = \left| R_{t-1}^{UU}(x-1)c_U(x-1, t-1) \right|^2 + \left| R_{t-1}^{UD}(x-1)c_D(x-1, t-1) \right|^2$$
$$+ \left| R_{t-1}^{DU}(x+1)c_U(x+1, t-1) \right|^2 + \left| R_{t-1}^{DD}(x+1)c_D(x+1, t-1) \right|^2 + f(x, t) + f^*(x, t), \tag{A11}$$

$$P_{\min}(x, t) = \left| R_{t-1}^{UU}(x-1)c_U(x-1, t-1) \right|^2 + \left| R_{t-1}^{UD}(x-1)c_D(x-1, t-1) \right|^2$$
$$+ \left| R_{t-1}^{DU}(x+1)c_U(x+1, t-1) \right|^2 + \left| R_{t-1}^{DD}(x+1)c_D(x+1, t-1) \right|^2 - f(x, t) - f^*(x, t). \tag{A12}$$

Therefore, the degree of interference will be given by

$$\mu_{x,t} = |4\,\mathrm{Re}(f(x,t))|. \tag{A13}$$

2. Degree of interference evolution

In this section, we move on to calculate the initial time steps of the evolution used to plot the degree of interference patterns in Fig. 6. In this evolution the coin operators used are $\hat{C}_H(\theta_H)$ and the identity operator $\hat{C}_F(\theta_F = 0) = \mathbb{I}_{2\times2}$. The initial state used is

$$\Psi_0 = |0\rangle \otimes \frac{|\uparrow\rangle + |\downarrow\rangle}{\sqrt{2}}. \tag{A14}$$

At time $t = 0$ the fractal pattern tells us that the coin operator is equal to $\hat{C}_H$ at $x = 0$ and the identity for $x \neq 0$. Therefore, after the application of the unitary operator we are going to have

$$\Psi_1 = \frac{(\cos\theta_H + \sin\theta_H)}{\sqrt{2}}|+1,\uparrow\rangle + \frac{(\sin\theta_H - \cos\theta_H)}{\sqrt{2}}|-1,\downarrow\rangle. \tag{A15}$$

For $t = 1$, the coin operator follows $\hat{R}_1 = \{\hat{C}_H, x = \pm1; \mathbb{I}, x \neq \pm1\}$. Then, by applying it to the state following with the application of the shift operator,

$$\Psi_2 = \frac{\cos\theta_H}{\sqrt{2}}(\cos\theta_H + \sin\theta_H)|+2,\uparrow\rangle + \frac{\sin\theta_H}{\sqrt{2}}|0\rangle \otimes [(\sin\theta_H - \cos\theta_H)|\uparrow\rangle + (\cos\theta_H + \sin\theta_H)|\downarrow\rangle]$$
$$- \frac{\cos\theta_H}{\sqrt{2}}(\sin\theta_H - \cos\theta_H)|-2,\downarrow\rangle.$$

When $t = 2$ and 3, $\hat{R}_2 = \{\hat{C}_H, x = \pm2; \mathbb{I}, x \neq \pm2\}$ and $\hat{R}_3 = \{\hat{C}_H, x = \pm1, \pm3; \mathbb{I}, x \neq \pm1, \pm3\}$. The states at these times are, respectively,

$$\Psi_3 = \frac{\cos^2\theta_H}{\sqrt{2}}(\cos\theta_H + \sin\theta_H)|+3,\uparrow\rangle + \frac{\cos^2\theta_H}{\sqrt{2}}(\sin\theta_H - \cos\theta_H)|-3,\downarrow\rangle$$
$$+ \frac{\sin\theta_H}{\sqrt{2}}|+1\rangle \otimes [(\sin\theta_H - \cos\theta_H)|\uparrow\rangle + \cos\theta_H(\cos\theta_H + \sin\theta_H)|\downarrow\rangle]$$
$$- \frac{\sin\theta_H}{\sqrt{2}}|-1\rangle \otimes [\cos\theta(\sin\theta_H - \cos\theta_H)|\uparrow\rangle - (\cos\theta_H + \sin\theta_H)|\downarrow\rangle],$$

$$\Psi_4 = \frac{\cos^3\theta_H}{\sqrt{2}}(\cos\theta_H + \sin\theta_H)|+4,\uparrow\rangle - \frac{\cos^3\theta_H}{\sqrt{2}}(\sin\theta_H - \cos\theta_H)|-4,\downarrow\rangle$$
$$+ \frac{\sin\theta_H}{\sqrt{2}}\cos\theta_H|+2\rangle \otimes \{[\sin\theta_H(1 + \sin\theta_H) + \cos\theta_H(\sin\theta_H - 1)]|\uparrow\rangle + \cos\theta_H(\cos\theta_H + \sin\theta_H)|\downarrow\rangle\}$$
$$+ \frac{\sin\theta_H}{\sqrt{2}}|0\rangle \otimes \{[\sin\theta_H(\cos\theta_H + \sin\theta_H) - \cos^2\theta_H(\sin\theta_H - \cos\theta_H)]|\uparrow\rangle$$
$$+ [\sin\theta_H(\sin\theta_H - \cos\theta_H) - \cos^2\theta_H(\cos\theta_H + \sin\theta_H)]|\downarrow\rangle\}$$
$$+ \frac{\sin\theta_H}{\sqrt{2}}\cos\theta_H|-2\rangle \otimes \{\cos\theta_H(\sin\theta_H - \cos\theta_H)|\uparrow\rangle - [\sin\theta_H(\sin\theta_H + 1) + \cos\theta_H(\sin\theta_H - 1)]|\downarrow\rangle\}.$$

Now we are going to use these states and the coin operators defined for each time step to calculate the degree of interference. At $t = 0$, as we do not have a previous time step, we set the interference degree to be equal to one at the origin:

$$\mu(x, 0) = \begin{cases} 1, & x = 0 \\ 0, & x \neq 0. \end{cases} \tag{A16}$$

At $t = 1$, we recall that for the degree of interference to be nonzero at a given position the coin operator applied in its immediate neighbors must be $\hat{C}_H$ and the coin has to be in a superposition as well. For $x = \pm1$ these requirements are

satisfied since the initial state located at the origin is in a superposition and $\hat{C}_H$ was applied. Then, we obtain

$$\mu(x, 1) = \begin{cases} 2\sin\theta_H\cos\theta_H, & x = \pm1 \\ 0, & x \neq \pm1. \end{cases} \tag{A17}$$

In the next time step, $t = 2$, given that the state is an entangled one, the requirement of having a superposition of coin states in a position is not fulfilled. Therefore, the interference degree is zero for every position:

$$\mu(x, 2) = 0, \ \forall \ x. \tag{A18}$$

Here we can already notice a difference between the degree of interference pattern and the Sierpinski-gasket fractal.

For $t = 3$ the same happens, however, for the reason that at $x = 0$ the coin operator used is the identity, while at $x = \pm 2$ $\hat{C}_H$ is used but the coin states are not in superposition:

$$\mu(x, 3) = 0, \ \forall \, x. \tag{A19}$$

At $t = 4$ we have to look at the walker state and the coin operator at $t = 3$. We notice that at $x = \pm 1$ the coin state is in a superposition and the identity is not applied at these positions. Therefore, the only points that the interference degree can be nonzero are at $x = 0$ and ± 2. Performing the calculations, we

find

$$\mu(x, 4) = \begin{cases} 4 \cos^2 \theta_H \sin^3 \theta_H \cos 2\theta_H, \ x = 0 \\ 2 \cos^2 \theta_H \sin^3 \theta_H \cos 2\theta_H, \ x = \pm 2 \\ 0, \ x \neq 0, \pm 2. \end{cases} \tag{A20}$$

Taking one more final step, $t = 5$, we find once again that the interference degree is zero for every position given that identity operator is applied to every position but at $x = \pm 4$, however, the coin state at these positions is not in superposition:

$$\mu(x, 5) = 0, \ \forall \, x. \tag{A21}$$

[1] B. B. Mandelbrot, *The Fractal Geometry of Nature*, Vol. 173 (WH Freeman, New York, 1983).

[2] J. L. Véhel, E. Lutton, and C. Tricot, *Fractals in Engineering: From Theory to Industrial Applications* (Springer, New York, 2012).

[3] A. Bunde and S. Havlin, *Fractals in Science* (Springer, Berlin, 2013).

[4] G. R. Newkome, P. Wang, C. N. Moorefield, T. J. Cho, P. P. Mohapatra, S. Li, S.-H. Hwang, O. Lukoyanova, L. Echegoyen, J. A. Palagallo *et al.*, Nanoassembly of a fractal polymer: A molecular "Sierpinski Hexagonal Gasket", Science **312**, 1782 (2006).

[5] J. A. Fan, W.-H. Yeo, Y. Su, Y. Hattori, W. Lee, S.-Y. Jung, Y. Zhang, Z. Liu, H. Cheng, L. Falgout *et al.*, Fractal design concepts for stretchable electronics, Nat. Commun. **5**, 3266 (2014).

[6] J. Shang, Y. Wang, M. Chen, J. Dai, X. Zhou, J. Kuttner, G. Hilt, X. Shao, J. M. Gottfried, and K. Wu, Assembling molecular Sierpiński triangle fractals, Nat. Chem. **7**, 389 (2015).

[7] S. N. Kempkes, M. R. Slot, S. E. Freeney, S. J. Zevenhuizen, D. Vanmaekelbergh, I. Swart, and C. M. Smith, Design and characterization of electrons in a fractal geometry, Nat. Phys. **15**, 127 (2019).

[8] Y. Aharonov, L. Davidovich, and N. Zagury, Quantum random walks, Phys. Rev. A **48**, 1687 (1993).

[9] R. Vieira, E. P. M. Amorim, and G. Rigolin, Dynamically disordered quantum walk as a maximal entanglement generator, Phys. Rev. Lett. **111**, 180503 (2013).

[10] C. M. Chandrashekar, Disorder induced localization and enhancement of entanglement in one- and two-dimensional quantum walks, arXiv:1212.5984.

[11] T. Chen and X. Zhang, The defect-induced localization in many positions of the quantum random walk, Sci. Rep. **6**, 25767 (2016).

[12] C. Ampadu, Return probability of the open quantum random walk with time-dependence, Commun. Theor. Phys. **59**, 563 (2013).

[13] M. A. Pires and S. M. D. Queirós, Parrondo's paradox in quantum walks with time-dependent coin operators, Phys. Rev. E **102**, 042124 (2020).

[14] M. A. Pires and S. M. Duarte Queirós, Negative correlations

can play a positive role in disordered quantum walks, Sci. Rep. **11**, 4527 (2021).

[15] X.-X. Fang, K. An, B.-T. Zhang, B. C. Sanders, and H. Lu, Maximal coin-position entanglement generation in a quantum walk for the third step and beyond regardless of the initial state, Phys. Rev. A **107**, 012433 (2023).

[16] H. Lavička, V. Potoček, T. Kiss, E. Lutz, and I. Jex, Quantum walk with jumps, Eur. Phys. J. D **64**, 119 (2011).

[17] G. Di Molfetta, D. O. Soares-Pinto, and S. M. D. Queirós, Elephant quantum walk, Phys. Rev. A **97**, 062112 (2018).

[18] M. A. Pires, G. Di Molfetta, and S. M. D. Queirós, Multiple transitions between normal and hyperballistic diffusion in quantum walks with time-dependent jumps, Sci. Rep. **9**, 19292 (2019).

[19] M. A. Pires and S. M. D. Queirós, Quantum walks with sequential aperiodic jumps, Phys. Rev. E **102**, 012104 (2020).

[20] A. Zaman, R. Ahmad, S. Bibi, and S. Khan, Randomizing quantum walk, Int. J. Theor. Phys. **61**, 135 (2022).

[21] C. B. Naves, M. A. Pires, D. O. Soares-Pinto, and S. M. D. Queirós, Quantum walks in two dimensions: Controlling directional spreading with entangling coins and tunable disordered step operator, J. Phys. A: Math. Theor. **56**, 125301 (2023).

[22] C. B. Naves, M. A. Pires, D. O. Soares-Pinto, and S. M. D. Queirós, Enhancing entanglement with the generalized elephant quantum walk from localized and delocalized states, Phys. Rev. A **106**, 042408 (2022).

[23] M. C. Bañuls, C. Navarrete, A. Pérez, E. Roldán, and J. C. Soriano, Quantum walk with a time-dependent coin, Phys. Rev. A **73**, 062304 (2006).

[24] S. Dhar, A. Khaleque, and T. K. Bose, Diverse tunable dynamics of two quantum random walkers, arXiv:1909.08527.

[25] P. Xue, R. Zhang, H. Qin, X. Zhan, Z. H. Bian, J. Li, and B. C. Sanders, Experimental quantum-walk revival with a time-dependent coin, Phys. Rev. Lett. **114**, 140502 (2015).

[26] A. Romanelli, Driving quantum-walk spreading with the coin operator, Phys. Rev. A **80**, 042332 (2009).

[27] T. Machida and N. Konno, Limit theorem for a time-dependent coined quantum walk on the line, in *Natural Computing* (Springer, Berlin, 2010), pp. 226–235.

[28] S. Panahiyan and S. Fritzsche, Simulation of the multiphase configuration and phase transitions with quantum walks utilizing a step-dependent coin, Phys. Rev. A **100**, 062115 (2019).

[29] N. Konno, Localization of an inhomogeneous discrete-time quantum walk on the line, Quantum Inf. Proc. **9**, 405 (2010).

[30] Z. J. Li, J. A. Izaac, and J. B. Wang, Position-defect-induced reflection, trapping, transmission, and resonance in quantum walks, Phys. Rev. A **87**, 012314 (2013).

[31] R. Zhang, P. Xue, and J. Twamley, One-dimensional quantum walks with single-point phase defects, Phys. Rev. A **89**, 042317 (2014).

[32] M. J. Cantero, F. Grünbaum, L. Moral, and L. Velázquez, One-dimensional quantum walks with one defect, Rev. Math. Phys. **24**, 1250002 (2012).

[33] A. R. C. Buarque and W. S. Dias, Aperiodic space-inhomogeneous quantum walks: Localization properties, energy spectra, and enhancement of entanglement, Phys. Rev. E **100**, 032106 (2019).

[34] R. Ahmad, U. Sajjad, and M. Sajid, One-dimensional quantum walks with a position-dependent coin, Commun. Theor. Phys. **72**, 065101 (2020).

[35] A. Ahlbrecht, C. Cedzich, R. Matjeschk, V. B. Scholz, A. H. Werner, and R. F. Werner, Asymptotic behavior of quantum walks with spatio-temporal coin fluctuations, Quantum Inf. Proc. **11**, 1219 (2012).

[36] R. Vieira, E. P. M. Amorim, and G. Rigolin, Entangling power of disordered quantum walks, Phys. Rev. A **89**, 042307 (2014).

[37] M. Montero, Quantum and random walks as universal generators of probability distributions, Phys. Rev. A **95**, 062326 (2017).

[38] M. Montero, Classical-like behavior in quantum walks with inhomogeneous, time-dependent coin operators, Phys. Rev. A **93**, 062316 (2016).

[39] Y. Shikano and H. Katsura, Localization and fractality in inhomogeneous quantum walks with self-duality, Phys. Rev. E **82**, 031122 (2010).

[40] C. Cedzich, J. Fillman, T. Geib, and A. Werner, Singular continuous cantor spectrum for magnetic quantum walks, Lett. Math. Phys. **110**, 1141 (2020).

[41] E. Agliari, A. Blumen, and O. Mülken, Quantum-walk approach to searching on fractal structures, Phys. Rev. A **82**, 012305 (2010).

[42] S. D. Berry and J. B. Wang, Quantum-walk-based search and centrality, Phys. Rev. A **82**, 042333 (2010).

[43] A. Patel and K. S. Raghunathan, Search on a fractal lattice using a quantum random walk, Phys. Rev. A **86**, 012332 (2012).

[44] S. Tamegai, S. Watabe, and T. Nikuni, Spatial search on Sierpinski Carpet using Quantum Walk, J. Phys. Soc. Jpn. **87**, 085003 (2018).

[45] R. Sato, T. Nikuni, and S. Watabe, Scaling hypothesis of a spatial search on fractal lattices using a quantum walk, Phys. Rev. A **101**, 022312 (2020).

[46] X.-Y. Xu, X.-W. Wang, D.-Y. Chen, C. M. Smith, and X.-M. Jin, Quantum transport in fractal networks, Nat. Photonics **15**, 703 (2021).

[47] P. C. S. Lara, R. Portugal, and S. Boettcher, Quantum walks on Sierpinski gaskets, Int. J. Quantum Inf. **11**, 1350069 (2013).

[48] R. F. S. Andrade and A. M. C. Souza, Discrete-time quantum walks generated by aperiodic fractal sequence of space coin operators, Int. J. Mod. Phys. C **29**, 1850098 (2018).

[49] E. Agliari, A. Blumen, and O. Mülken, Dynamics of continuous-time quantum walks in restricted geometries, J. Phys. A: Math. Theor. **41**, 445301 (2008).

[50] Z. Darázs, A. Anishchenko, T. Kiss, A. Blumen, and O. Mülken, Transport properties of continuous-time quantum walks on Sierpinski fractals, Phys. Rev. E **90**, 032113 (2014).

[51] A. Bunde and S. Havlin, *Fractals and Disordered Systems* (Springer, New York, 2012).

[52] O. Martin, A. M. Odlyzko, and S. Wolfram, Algebraic properties of cellular automata, Commun. Math. Phys. **93**, 219 (1984).

[53] D. Ettestad and J. Carbonara, Distinguishing between Sierpinski triangle constructions, Fractals **27**, 1950091 (2019).

[54] J. Nagler and J. C. Claussen, $1/f^\alpha$ spectra in elementary cellular automata and fractal signals, Phys. Rev. E **71**, 067103 (2005).

[55] A. Schreiber, K. N. Cassemiro, V. Potoček, A. Gábris, I. Jex, and C. Silberhorn, Photons walking the line: a quantum walk with adjustable coin operations, Phys. Rev. Lett. **106**, 180403 (2011).

[56] Q.-Q. Wang, X.-Y. Xu, W.-W. Pan, K. Sun, J.-S. Xu, G. Chen, Y.-J. Han, C.-F. Li, and G.-C. Guo, Dynamic-disorder-induced enhancement of entanglement in photonic quantum walks, Optica **5**, 1136 (2018).

[57] A. Nayak and A. Vishwanath, Quantum Walk on the Line, arXiv:quant-ph/0010117.

[58] A. Ambainis, E. Bach, A. Nayak, A. Vishwanath, and J. Watrous, One-dimensional quantum walks, *Proceedings of the Annual ACM Symposium on Theory of Computing* (ACM, New York, 2001), p. 37.

[59] E. Bach, S. Coppersmith, M. P. Goldschen, R. Joynt, and J. Watrous, One-dimensional quantum walks with absorbing boundaries, J. Comput. Syst. Sci. **69**, 562 (2004).

[60] L. Levi, Y. Krivolapov, S. Fishman, and M. Segev, Hyper-transport of light and stochastic acceleration by evolving disorder, Nat. Phys. **8**, 912 (2012).

[61] F. A. Oliveira, R. M. S. Ferreira, L. C. Lapas, and M. H. Vainstein, Anomalous diffusion: A basic mechanism for the evolution of inhomogeneous systems, Front. Phys. **7**, 18 (2019).

[62] A. C. Orthey and E. P. Amorim, Weak disorder enhancing the production of entanglement in quantum walks, Braz. J. Phys. **49**, 595 (2019).

[63] B. Abd-El-Atty, A. A. Abd El-Latif, and S. E. Venegas-Andraca, An encryption protocol for NEQR images based on one-particle quantum walks on a circle, Quantum Inf. Proc. **18**, 272 (2019).

[64] M. Segev, M. Soljačić, and J. M. Dudley, Fractal optics and beyond, Nat. Photon. **6**, 209 (2012).

[65] O. Graydon, Fractal behaviour, Nat. Photon. **13**, 228 (2019).

[66] D. S. Wiersma, Disordered photonics, Nat. Photon. **7**, 188 (2013).